Progress of Theoretical Physics, Vol. 96, No. 4, October 1996

Innermost Stable Circular Orbit of Coalescing Neutron Star-Black Hole Binary

—— Generalized Pseudo-Newtonian Potential Approach ——

Keisuke TANIGUCHI and Takashi NAKAMURA*

Department of Physics, Kyoto University, Kyoto 606-01
**Yukawa Institute for Theoretical Physics, Kyoto University, Kyoto 606-01*

(Received June 21, 1996)

The innermost stable circular orbits (ISCO) of coalescing neutron star-black hole binaries are studied taking into account both tidal and relativistic effects. We adopt the generalized pseudo-Newtonian potential to mimic the general relativistic effects of gravitation. It is found that the separation of the neutron star and the black hole at the innermost stable circular orbit is greater than that obtained by using either the Newtonian potential (i.e., the case in which only the tidal interaction is included) or the second post-Newtonian equation of motion of a point mass (i.e., the case in which the effect of general relativity is taken into account but the tidal force is neglected). In equal mass cases, it is found that for $\bar{a}/m_1 \gtrsim 3.5$ with $\bar{a}$ and m_1 being the mean radius and the mass of the neutron star, the tidal effect dominates the stability of the binary system, while for $\bar{a}/m_1 \lesssim 3.5$, the relativistic effect, i.e., the fact that the interaction potential has an unstable orbit, does. The effect of the circulation is also studied by comparing the Roche ellipsoids (REs) with the irrotational Roche-Riemann ellipsoids (IRREs). In the IRREs case, which are believed to be the case of coalescing binary neutron stars, it is found that in the equal mass binary case, the orbital frequency is 495 Hz at the ISCO.

§ 1. Introduction

Laser interferometers for example LIGO,[1] VIRGO,[2] GEO[3] and TAMA,[4] are currently being constructed and the detection of gravitational waves is expected at the end of this century. One of the most important sources of gravitational waves for these detectors is coalescing binary compact stars such as NS-NS, NS-BH and BH-BH binaries. Each mass, each spin and the distance of the binary can be determined by applying matched filter techniques[5] to the gravitational wave form of the so-called last three minutes of the binary.[6] In the end of the last three minutes, two compact stars coalesce, and the nonlinear character of the gravity and the tidal effects become important. This will be the most exciting part of the coalescing event.

It is known from the study of orbits of a test particle in the Schwarzschild metric that the innermost stable circular orbit (ISCO) exists at $r=6M$. For binary cases, Kidder, Will, and Wiseman[7] investigated a point-mass binary using a second post-Newtonian equation of motion, and found that the ISCO of the comparable mass binary is at $r_{gr} \simeq 7M_{\rm tot}$, where r_{gr} is the separation of the binary in the Schwarzschild like radial coordinate.

As for the tidal effects, Chandrasekhar[8] studied the Roche limit by using Newtonian gravity and treating binary systems as incompressible homogeneous ellipsoids. He found that the stars are tidally disrupted before contact at $r_t = (2.25M_{\rm tot}/\rho)^{1/3}$ for equal mass binary, where ρ is the constant density of ellipsoids. For the typical neutron star with $M_{\rm tot}=2.8M_\odot$ and $\rho=1\times10^{15}{\rm g/cm^3}$, r_t becomes

$5.6M_{\rm tot}$.

Recently Lai, Rasio and Shapiro[9),10)] have investigated binaries consisting of finite size compressible stars using approximate equilibria. In a series of papers, they took into account the effect of the quadrupole order deviation of stars and found that the hydrodynamic instability occurs at $r_h=6\sim7.5M_{\rm tot}$ for $n=0.5$ polytropic neutron star with the radius $R_0=2.5M_{\rm tot}$.

In order to know at what radius the final merging phase begins, all three effects, that is, the general relativistic, tidal and hydrodynamic effects should be taken into account simultaneously since r_{gr}, r_t and r_h have similar values of $\sim7M_{\rm tot}$. For this purpose we must solve the fully general relativistic equations, which is a difficult 3D problem in numerical relativity,[11)] although the partly general relativistic results have already been presented.[12),13)] To know the qualitative feature of the ISCOs we will use various approximations to calculate equilibria of the binary in this paper. The reward is that all the calculations can be done analytically, so that our results will contribute some physical insight to the final understanding of the ISCO.

In this paper, we will solve the Roche problem [8)] as a model of a binary that consists of a finite size star and a point-like gravity source. A gravitational potential which has unstable circular orbits will be used as an interaction potential of the binary. Specifically, we generalize the pseudo-Newtonian potential proposed by Paczyński and Wiita[14)] to mimic general relativistic effects. We belive that this model mimics a neutron star-black hole binary and describes its qualitative behavior.

This paper is organized as follows. In § 2 the basic equation necessary for constructing equilibrium configurations of the Roche ellipsoids (REs) and the Roche-Riemann ellipsoids (RREs)[15)] are derived in the case of a general interaction potential. In § 3 circular orbits of the neutron star-black hole binary are calculated using the generalized pseudo-Newtonian potential to mimic the effects of general relativity, and the results are shown in § 4. In § 5 our results are compared with those using the Newtonian potential and the second order post-Newtonian equation of motion. We use the units $c=G=1$ throughout this paper.

§ 2. Generalized Roche-Riemann ellipsoids

We first regard the black hole as a point particle of mass m_2 and denote the gravitational potential by the black hole as $V_2(r)$. To mimic the effects of general relativity by $V_2(r)$, we do not fix the form of $V_2(r)$ at the moment. Next we treat the neutron star as an incompressible, homogeneous ellipsoid of the semi-axes a_1, a_2 and a_3, mass m_1 and the density ρ_1. We treat the self-gravity of the neutron star (V_1) as Newtonian. Although for mathematical convenience we assume incompressibility for the equation of state, the effect of the compressibility can be easily taken into account in an approximate way.[9)] Following Chandrasekhar,[8)] we call the neutron star the 'primary' and the black hole the 'secondary'.

A. *Second virial equations*

We use the tensor virial method,[8)] and derive the equations necessary for constructing equilibrium figures of this system. Choose a coordinate system such that

the origin is at the center of mass of the primary, the x_1-axis points to the center of mass of the secondary, and x_3-axis coincides with the direction of the angular velocity of the binary Ω. In the frame of reference rotating with Ω, the Euler equations of the primary are written as

$$\rho_1\frac{du_i}{dt}=-\frac{\partial P}{\partial x_i}+\rho_1\frac{\partial}{\partial x_i}\left[V_1+V_2+\frac{1}{2}\Omega^2\left\{\left(\frac{m_2R}{m_1+m_2}-x_1\right)^2+x_2^2\right\}\right]+2\rho_1\Omega\epsilon_{il3}u_l\,, \tag{2·1}$$

where ρ_1, u_i, P and R are the density, the internal velocity, the pressure and the separation between the neutron star and the black hole, respectively.

Let us expand the interaction potential V_2 in power series of x_k up to the second order. This approximation is justified if R is much larger than a_1, a_2 and a_3. We assume that the potential V_2 is spherically symmetric so that it depends only on the distance r from the center of mass of the secondary as

$$V_2=V_2(r)\,, \tag{2·2}$$

where r is given by

$$r=\{(R-x_1)^2+x_2^2+x_3^2\}^{1/2}\,. \tag{2·3}$$

The expansion of $V_2(r)$ becomes

$$V_2=(V_2)_0-\left(\frac{\partial V_2}{\partial r}\right)_0x_1+\frac{1}{2}\left(\frac{\partial^2V_2}{\partial r^2}\right)_0x_1^2+\frac{1}{2R}\left(\frac{\partial V_2}{\partial r}\right)_0(x_2^2+x_3^2)\,, \tag{2·4}$$

where the subscript 0 denotes the derivatives at the origin of the coordinates. In the case of a circular orbit, we have from the force balance at the center

$$\frac{m_2R}{m_1+m_2}\Omega^2=-\left(\frac{\partial V_2}{\partial r}\right)_0(1+\delta)\,, \tag{2·5}$$

where δ is the quadrupole term of the interaction potential.[9]

Substituting Eqs. (2·4) and (2·5) into Eq. (2·1), we have

$$\rho_1\frac{du_i}{dt}=-\frac{\partial P}{\partial x_i}+\rho_1\frac{\partial}{\partial x_i}\left[V_1+\delta\left(\frac{\partial V_2}{\partial r}\right)_0x_1+\frac{1}{2}\Omega^2(x_1^2+x_2^2)+\frac{1}{2}\left(\frac{\partial^2V_2}{\partial r^2}\right)_0x_1^2\right.$$
$$\left.+\frac{1}{2R}\left(\frac{\partial V_2}{\partial r}\right)_0(x_2^2+x_3^2)\right]+2\rho_1\Omega\epsilon_{il3}u_l\,. \tag{2·6}$$

Multiplying x_j to Eq. (2·6) and integrating over the volume of the primary, we have

$$\frac{d}{dt}\int\rho_1u_ix_jd^3\boldsymbol{x}=2T_{ij}+W_{ij}+\left\{\Omega^2+\left(\frac{\partial^2V_2}{\partial r^2}\right)_0\right\}\delta_{1i}I_{1j}$$
$$+\left\{\Omega^2+\frac{1}{R}\left(\frac{\partial V_2}{\partial r}\right)_0\right\}\delta_{2i}I_{2j}+\frac{1}{R}\left(\frac{\partial V_2}{\partial r}\right)_0\delta_{3i}I_{3j}$$
$$+2\Omega\epsilon_{il3}\int\rho_1u_lx_jd^3\boldsymbol{x}+\delta_{ij}\Pi\,, \tag{2·7}$$

where

$$T_{ij}\equiv\frac{1}{2}\int\rho_1 u_i u_j d^3\boldsymbol{x}: \text{ Kinetic Energy Tensor}, \tag{2·8}$$

$$W_{ij}\equiv\int\rho_1\frac{\partial V_1}{\partial x_i}x_j d^3\boldsymbol{x}: \text{ Potential Energy Tensor}, \tag{2·9}$$

$$I_{ij}\equiv\int\rho_1 x_i x_j d^3\boldsymbol{x}: \text{ Moment of Inertia Tensor} \tag{2·10}$$

and

$$\Pi\equiv\int P d^3\boldsymbol{x}. \tag{2·11}$$

In Eq. (2·7) there are no terms related to δ. Since it is possible to take the coordinate system comoving with the center of mass of the binary system, the term proportional to δ in Eq. (2·6) vanishes when we integrate over the volume of the primary. Equation (2·7) is the basic equation to construct the equilibrium figures of the Roche ellipsoids (REs) and the Roche-Riemann ellipsoids (RREs) for the general potential $V_2(r)$.

B. *Equilibrium Roche-Riemann sequence*

In this subsection, we show how to construct the equilibrium figures of the RREs. The Roche-Riemann ellipsoid is the equilibrium in which the shape of the primary does not change in the rotating frame although the uniform vorticity exists inside the primary. We restrict the problem to the simplest case, where the uniform vorticity of the primary is parallel to the rotation axis, i.e., the primary is the Riemann S-type ellipsoid.[8]

We set the coordinate axes to coincide with the principal axes of the primary. For the uniform vorticity ζ, the internal velocity u_i in the rotating frame is given by

$$u_1=Q_1 x_2, \tag{2·12}$$

$$u_2=Q_2 x_1 \tag{2·13}$$

and

$$u_3=0, \tag{2·14}$$

where

$$Q_1=-\frac{{a_1}^2}{{a_1}^2+{a_2}^2}\zeta \tag{2·15}$$

and

$$Q_2=\frac{{a_2}^2}{{a_1}^2+{a_2}^2}\zeta. \tag{2·16}$$

For the stationary equilibrium, Eq. (2·7) is rewritten as

$$Q_{ik}Q_{jl}I_{kl}+W_{ij}+\left\{\Omega^2+\left(\frac{\partial^2 V_2}{\partial r^2}\right)_0\right\}\delta_{1i}I_{1j}+\left\{\Omega^2+\frac{1}{R}\left(\frac{\partial V_2}{\partial r}\right)_0\right\}\delta_{2i}I_{2j}$$

$$+\frac{1}{R}\left(\frac{\partial V_2}{\partial r}\right)_0\delta_{3i}I_{3j}+2\Omega\epsilon_{il3}Q_{lk}I_{kj}=-\delta_{ij}\Pi\,, \tag{2·17}$$

where Q_{ij} is non-zero only for

$$Q_{12}=Q_1\,, \tag{2·18}$$

$$Q_{21}=Q_2\,. \tag{2·19}$$

Equation (2·17) has only diagonal components:

$$Q_1{}^2I_{22}+W_{11}+\left\{\Omega^2+\left(\frac{\partial^2 V_2}{\partial r^2}\right)_0\right\}I_{11}+2\Omega Q_2I_{11}=-\Pi\,, \tag{2·20}$$

$$Q_2{}^2I_{11}+W_{22}+\left\{\Omega^2+\frac{1}{R}\left(\frac{\partial V_2}{\partial r}\right)_0\right\}I_{22}-2\Omega Q_1I_{22}=-\Pi \tag{2·21}$$

and

$$W_{33}+\frac{1}{R}\left(\frac{\partial V_2}{\partial r}\right)_0I_{33}=-\Pi\,. \tag{2·22}$$

We assume for simplicity that the gravitational potential of the primary is Newtonian. In this case, the potential energy tensor and the moment of inertia tensor of the incompressible, homogeneous ellipsoids are calculated as

$$W_{ij}=-2\pi\rho_1A_iI_{ij} \tag{2·23}$$

and

$$I_{ij}=\frac{1}{5}m_1a_i{}^2\delta_{ij}\,, \tag{2·24}$$

where

$$A_i=a_1a_2a_3\int_0^\infty\frac{du}{\Delta(a_i{}^2+u)}\,, \tag{2·25}$$

and

$$\Delta^2=(a_1{}^2+u)(a_2{}^2+u)(a_3{}^2+u)\,. \tag{2·26}$$

Eliminating Π from Eqs. (2·20)~(2·22), we have

$$\left[\left\{1+2\frac{a_2{}^2}{a_1{}^2+a_2{}^2}f_R+\left(\frac{a_1a_2}{a_1{}^2+a_2{}^2}f_R\right)^2\right\}\Omega^2+\left(\frac{\partial^2 V_2}{\partial r^2}\right)_0\right]a_1{}^2-\frac{1}{R}\left(\frac{\partial V_2}{\partial r}\right)_0a_3{}^2$$
$$=2\pi\rho_1(a_1{}^2-a_3{}^2)B_{13} \tag{2·27}$$

and

$$\left[\left\{1+2\frac{a_1{}^2}{a_1{}^2+a_2{}^2}f_R+\left(\frac{a_1a_2}{a_1{}^2+a_2{}^2}f_R\right)^2\right\}\Omega^2+\frac{1}{R}\left(\frac{\partial V_2}{\partial r}\right)_0\right]a_2{}^2-\frac{1}{R}\left(\frac{\partial V_2}{\partial r}\right)_0a_3{}^2$$
$$=2\pi\rho_1(a_2{}^2-a_3{}^2)B_{23}\,, \tag{2·28}$$

where

$$f_R \equiv \frac{\zeta}{\Omega} \tag{2·29}$$

and the following relations are used,

$$a_i^2 A_i - a_j^2 A_j = (a_i^2 - a_j^2) B_{ij}\,, \tag{2·30}$$

where

$$B_{ij} = a_1 a_2 a_3 \int_0^\infty \frac{du}{\Delta (a_i^2+u)(a_j^2+u)}\,. \tag{2·31}$$

Now from Eq. (2·5) Ω is given by

$$\Omega^2 = -\frac{1+p}{R}\left(\frac{\partial V_2}{\partial r}\right)_0 (1+\delta)\,. \quad \left(p \equiv \frac{m_1}{m_2}\right) \tag{2·32}$$

Dividing Eq. (2·27) by Eq. (2·28), we have the equation to determine the Roche-Riemann sequences as

$$\frac{\left[(1+p)(1+\delta)\left\{1+2\frac{a_2^2}{a_1^2+a_2^2}f_R+\left(\frac{a_1 a_2}{a_1^2+a_2^2}f_R\right)^2\right\}-R\left(\frac{\partial^2 V_2}{\partial r^2}\right)_0\Big/\left(\frac{\partial V_2}{\partial r}\right)_0\right]a_1^2+a_3^2}{\left[(1+p)(1+\delta)\left\{1+2\frac{a_1^2}{a_1^2+a_2^2}f_R+\left(\frac{a_1 a_2}{a_1^2+a_2^2}f_R\right)^2\right\}-1\right]a_2^2+a_3^2}$$

$$= \frac{(a_1^2-a_3^2)B_{13}}{(a_2^2-a_3^2)B_{23}}\,. \tag{2·33}$$

Using Eqs. (2·28) and (2·32), we can determine the orbital angular velocity Ω by

$$\frac{\Omega^2}{\pi\rho_1} = \frac{2(1+p)(1+\delta)(a_2^2-a_3^2)B_{23}}{\left[(1+p)(1+\delta)\left\{1+2\frac{a_1^2}{a_1^2+a_2^2}f_R+\left(\frac{a_1 a_2}{a_1^2+a_2^2}f_R\right)^2\right\}-1\right]a_2^2+a_3^2}\,. \tag{2·34}$$

Note that f_R is related to the circulation C as

$$C = \oint \boldsymbol{u}_{\text{inertial}} \cdot d\boldsymbol{l} = \pi a_1 a_2 (2+f_R)\Omega\,, \tag{2·35}$$

where

$$\boldsymbol{u}_{\text{inertial}} = \begin{cases} (u_{\text{inertial}})_1 = (Q_1 - \Omega)x_2\,, \\ (u_{\text{inertial}})_2 = (Q_2+\Omega)x_1 - \dfrac{R}{1+p}\Omega\,, \\ (u_{\text{inertial}})_3 = 0\,. \end{cases} \tag{2·36}$$

If there is no viscosity inside the primary, the circulation should be conserved from Kelvin's circulation theorem.

C. *Total angular momentum*

The total energy and the total angular momentum of the binary are decreasing functions of time since gravitational waves are emitted. If the total angular momentum has its minimum at some separation of the binary, we regard this point as the

ISCO.*) The total angular momentum of our system, which is the sum of the orbital and the spin angular momenta is given by

$$J_{\rm tot}=m_1 r_{cm}^2\Omega+m_2(R-r_{cm})^2\Omega+I\Omega+\frac{2}{5}m_1\frac{a_1^2a_2^2}{a_1^2+a_2^2}\zeta$$

$$=\frac{m_1m_2}{m_1+m_2}R^2\Omega\left\{1+\frac{1}{5}(1+p)\frac{1}{R^2}\left(a_1^2+a_2^2+2\frac{a_1^2a_2^2}{a_1^2+a_2^2}f_R\right)\right\}, \tag{2·37}$$

where

$$r_{cm}=\frac{m_2R}{m_1+m_2}. \tag{2·38}$$

The first term in the braces of the right-hand side of Eq. (2·37) comes from the orbital angular momentum of the binary system and the second comes from the spin angular momentum of the primary.

§ 3. Generalized pseudo-Newtonian potential

There are variety of choices of $V_2(r)$ to mimic the general relativistic effects of gravitation. We generalize the so-called pseudo-Newtonian potential proposed by Paczyński and Wiita[14] originally. This potential fits the effective potential of the Schwarzschild black hole quite well, as we will show later. We will use the generalized pseudo-Newtonian potential defined by

$$V_2(r)=\frac{m_2}{r-r_{\rm pseudo}}, \tag{3·1}$$

$$r_{\rm pseudo}=r_s\{1+g(p)\}, \tag{3·2}$$

$$g(p)=\frac{7.49p}{6(1+p)^2}-\frac{10.4p^2}{3(1+p)^4}+\frac{29.3p^3}{6(1+p)^6}, \tag{3·3}$$

$$r_s\equiv\frac{2GM_{\rm tot}}{c^2}, \tag{3·4}$$

$$M_{\rm tot}=m_1+m_2, \tag{3·5}$$

where $p=m_1/m_2$ and $g(p)$ is the special term to fit the ISCOs of the hybrid second post-Newtonian calculations by Kidder, Will and Wiseman.[7] For $p=0$, the generalized pseudo-Newtonian potential agrees with the pseudo-Newtonian potential proposed by Paczyński and Wiita.[14]

Figure 1(a) shows effective potentials (solid lines) and locations of circular orbits (dots) in our generalized pseudo-Newtonian potential ($p=0$ and $r_{\rm pseudo}=r_s$) and in the Schwarzschild metric. Although by this choice of the parameter ($r_{\rm pseudo}=r_s$), the locations of the ISCOs in the generalized pseudo-Newtonian potential agree with

*) Lai, Rasio, and Shapiro showed in Appendix D of Ref. 9) that the true minimum point of the total energy coincides with that of the total angular momentum. Strictly speaking, if the rotation includes terms only to the quadrupole order, this coincidence fails. However, the difference is as small as the numerical accuracy.[9]

those in the Schwarzschild metric, the angular momenta at the ISCO are different, that is, the angular momentum in the generalized pseudo-Newtonian potential ($J_{\rm pseudo}$) for $p=0$ is $(9/8)^{1/2}$ times larger than that in the Schwarzschild metric ($J_{\rm Sch}$) at the ISCO. Therefore in Figs. 1(a) and (b) we compare circular orbits with different angular momenta related as

$$J_{\rm pseudo}=\left(\frac{9}{8}\right)^{1/2}J_{\rm Sch}\,. \tag{3·6}$$

From Fig. 1(b) we see that the radii of the circular orbits of the generalized pseudo-Newtonian potential agree with those of the effective potential around Schwarzschild black hole within 10 % accuracy near the ISCO. This is the reason we believe that our generalized pseudo-Newtonian potential expresses the effect of general relativity within 10 % or so.

Using Eqs. (3·1) and (2·32), we can rewrite Eq. (2·34) as

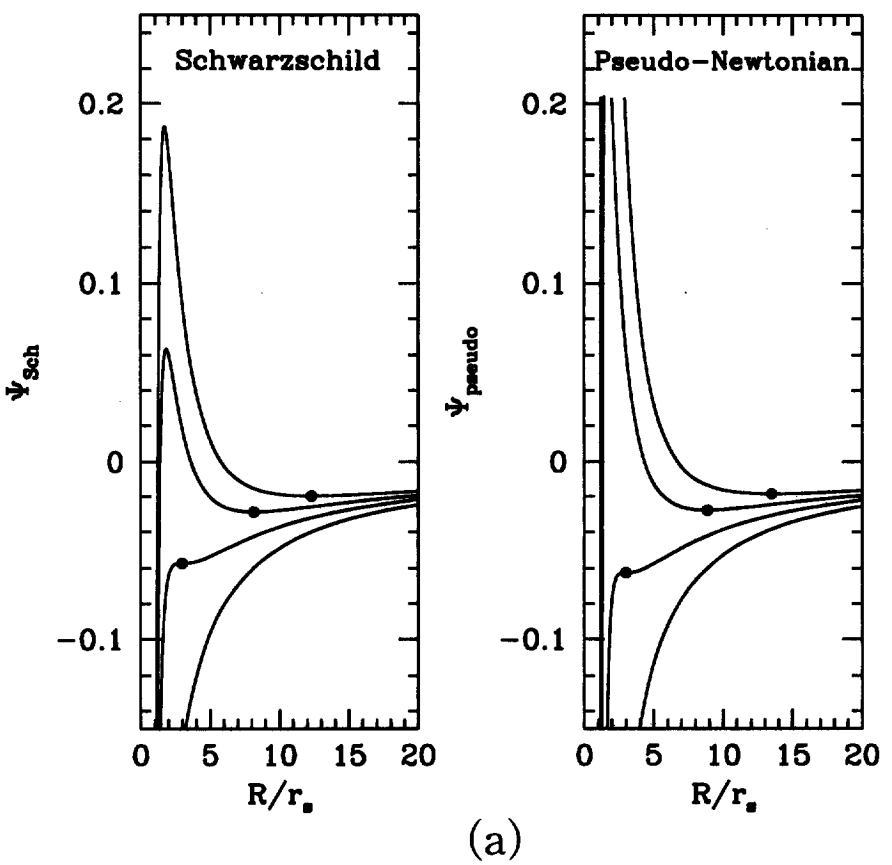

Fig. 1. (continued)

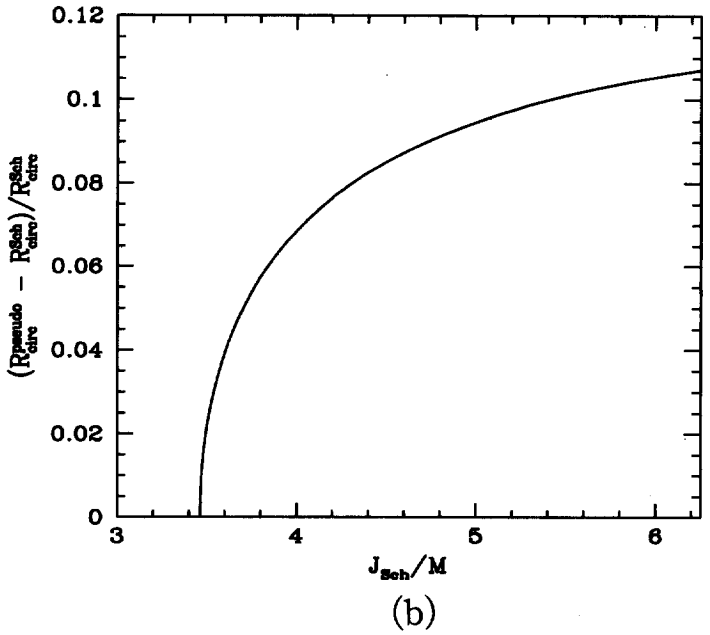

Fig. 1. (a) The effective potentials of a test particle in the Schwarzschild metric (left) and the pseudo-Newtonian potential (right) as a function of the normalized distance R/r_s. The vertical axes denote $\Psi_{Sch}=\sqrt{(1-(2M/R))((J^2_{Sch}/R^2)+1)}-1$ and $\Psi_{pseudo}=-(M/(R-r_s))+(J^2_{pseudo}/2R^2)$, respectively. The dots express the place of circular orbits. The value of the effective potential of the Schwarzschild black hole at the infinity is shifted to zero. (b) The fractional deviation of the circular orbits of the pseudo-Newtonian potential from those of the Schwarzschild effective potential as a function of the angular momentum. Circular orbits with different angular momentum related as $J_{pseudo}=(9/8)^{1/2}J_{Sch}$ are compared (see the text).

$$\frac{p^2 r_s{}^3(\bar{a}/m_1)^3}{12(1+p)^3R(R-r_{pseudo})^2} - \frac{(a_2{}^2-a_3{}^2)B_{23}}{\left[(1+p)(1+\delta)\left\{1+2\frac{a_1{}^2}{a_1{}^2+a_2{}^2}f_R+\left(\frac{a_1a_2}{a_1{}^2+a_2{}^2}f_R\right)^2\right\}-1\right]a_2{}^2+a_3{}^2}=0\,, \quad (3\cdot7)$$

where $\bar{a}$ is the mean radius of the primary. In the generalized pseudo-Newtonian case, the quadrupole term δ is written as

$$\delta=\frac{3}{10}\left\{2a_1{}^2-\frac{(3R-r_{pseudo})(R-r_{pseudo})}{3R^2}(a_2{}^2+a_3{}^2)\right\}\frac{1}{(R-r_{pseudo})^2}\,. \quad (3\cdot8)$$

We also have the separation of the binary as

$$R=\frac{E}{E-2}r_{pseudo}\,, \quad (3\cdot9)$$

where

$$E\equiv-(1+p)(1+\delta)\left\{1+2\frac{a_2^2}{a_1^2+a_2^2}f_R+\left(\frac{a_1a_2}{a_1^2+a_2^2}f_R\right)^2\right\}-\frac{a_3^2}{a_1^2}$$
$$+\left\{\left[(1+p)(1+\delta)\left\{1+2\frac{a_1^2}{a_1^2+a_2^2}f_R\right.\right.\right.$$
$$\left.\left.\left.+\left(\frac{a_1a_2}{a_1^2+a_2^2}f_R\right)^2\right\}-1\right]\frac{a_2^2}{a_1^2}+\frac{a_3^2}{a_1^2}\right\}\frac{(a_1^2-a_3^2)B_{13}}{(a_2^2-a_3^2)B_{23}}. \tag{3·10}$$

For the given mass ratio p, mean radius $\bar{a}/m_1$, circulation parameter f_R, and axial ratio a_3/a_1, we can determine the axial ratio a_2/a_1 by solving Eq. (3·7) with Eqs. (3·8) and (3·9). Using the axial ratios (a_2/a_1, a_3/a_1), we are able to calculate the orbital angular velocity by Eq. (2·34) and the separation of the binary by Eq. (3·9). The total angular momentum is calculated by Eq. (2·37). Finding the minimum of the total angular momentum, we can determine the location of the ISCO.

When the viscosity inside the primary is so effective that no internal motion exists, $f_R=0$ in the above equation, i.e., the Roche ellipsoids (REs) result. While if the primary is in-viscid and $C=0$, we have $f_R=-2$, i.e., the irrotational Roche-Riemann ellipsoids (IRREs) result. Note that if we substitute the Newtonian potential as an interaction potential, Eqs. (2·33) and (2·34) agree with the equations derived by Chandrasekhar[8] in the REs ($f_R=0$) case and those by Aizenman[15] in the RREs case.

Table I. Equilibrium sequences of the Roche ellipsoids (REs) and the irrotational Roche-Riemann ellipsoids (IRREs) with $p=1$ and $\bar{a}/m_1=3$.

$p=1$									
$\bar{a}/m_1=3$									
Roche Sequences					Irrotational Roche-Riemann Sequences				
a_3/a_1	a_2/a_1	$\tilde{\Omega}^2$	$\tilde{J}$	R/r_s	a_3/a_1	a_2/a_1	$\tilde{\Omega}^2$	$\tilde{J}$	R/r_s
0.950	0.966	1.87(−2)	2.97	4.75	0.950	0.948	2.69(−2)	2.87	4.31
					0.918	0.912	4.10(−2)	2.86	3.87†
0.912	0.939	3.19(−2)	2.94	4.13†					
0.900	0.929	3.59(−2)	2.94	4.00	0.900	0.891	4.81(−2)	2.86	3.72
0.850	0.889	5.19(−2)	2.97	3.65	0.850	0.833	6.53(−2)	2.88	3.46
0.800	0.847	6.67(−2)	3.01	3.44	0.800	0.773	7.92(−2)	2.92	3.31
0.750	0.801	8.03(−2)	3.05	3.30	0.750	0.715	9.02(−2)	2.95	3.22
0.700	0.754	9.23(−2)	3.10	3.21	0.700	0.657	9.87(−2)	3.00	3.17
0.650	0.704	1.03(−1)	3.15	3.14	0.650	0.601	1.05(−1)	3.04	3.14
0.600	0.652	1.11(−1)	3.20	3.10	0.600	0.547	1.09(−1)	3.09	3.12
					0.577	0.524	1.11(−1)	3.12	3.12‡
0.550	0.599	1.17(−1)	3.26	3.08	0.550	0.496	1.12(−1)	3.15	3.12
0.514	0.560	1.20(−1)	3.30	3.07‡					
0.500	0.544	1.21(−1)	3.32	3.07	0.500	0.447	1.12(−1)	3.21	3.14
0.450	0.489	1.22(−1)	3.38	3.09	0.450	0.400	1.11(−1)	3.28	3.17
0.400	0.433	1.19(−1)	3.45	3.12	0.400	0.354	1.07(−1)	3.36	3.21
0.350	0.376	1.14(−1)	3.53	3.18	0.350	0.310	1.02(−1)	3.45	3.28
0.300	0.320	1.05(−1)	3.63	3.27	0.300	0.267	9.33(−2)	3.56	3.37
0.250	0.264	9.17(−2)	3.75	3.41	0.250	0.225	8.23(−2)	3.69	3.51
0.200	0.209	7.53(−2)	3.90	3.62	0.200	0.182	6.83(−2)	3.86	3.72

§ 4. Results

Kochanek[16] and Bildsten and Cutler[17] showed that the internal structure of a coalescing binary neutron star is an irrotational Roche-Riemann ellipsoid (IRREs). However we calculate both the REs and the IRREs for comparison. We show the results in four cases; 1) the REs with $p=1$ and 0.1, 2) the IRREs with $p=1$ and 0.1. Results are given in Tables I~VI, where $\tilde{\Omega}=\Omega/\sqrt{\pi\rho_1}$ represents the normalized orbital angular velocity, and $\tilde{J}$ denotes the normalized total angular momentum defined by

$$\tilde{J}=\frac{J_{\rm tot}}{m_1 m_2 (r_s/M_{\rm tot})^{1/2}}\,. \tag{4·1}$$

Here, $\bar{a}$ is the mean radius of the primary defined by

$$\bar{a}=\left(\frac{m_1}{\frac{4}{3}\pi\rho_1}\right)^{1/3}\,. \tag{4·2}$$

In Tables I~VI, † denotes the point of the ISCO defined in this paper, and ‡ the point of the Roche limit where the Roche limit is defined by the distance of the closest approach for equilibrium to be possible.[8] The values in the parentheses show the power of 10.

Table II. Equilibrium sequences of the REs and the IRREs with $p=1$ and $\bar{a}/m_1=5$.

$p=1$									
$\bar{a}/m_1=5$									
Roche Sequences					Irrotational Roche-Riemann Sequences				
a_3/a_1	a_2/a_1	$\tilde{\Omega}^2$	$\tilde{J}$	R/r_s	a_3/a_1	a_2/a_1	$\tilde{\Omega}^2$	$\tilde{J}$	R/r_s
0.950	0.967	1.97(−2)	3.30	7.24	0.950	0.947	2.90(−2)	3.12	6.47
0.900	0.931	3.81(−2)	3.18	5.99	0.900	0.890	5.25(−2)	3.02	5.48
0.850	0.892	5.56(−2)	3.15	5.40	0.850	0.831	7.15(−2)	2.99	5.05
					0.832	0.810	7.73(−2)	2.99	4.95†
0.828	0.874	6.29(−2)	3.15	5.22†					
0.800	0.850	7.19(−2)	3.15	5.04	0.800	0.771	8.67(−2)	2.99	4.81
0.750	0.806	8.68(−2)	3.17	4.81	0.750	0.711	9.85(−2)	3.01	4.66
0.700	0.759	1.00(−1)	3.20	4.64	0.700	0.653	1.08(−1)	3.04	4.57
0.650	0.709	1.12(−1)	3.24	4.53	0.650	0.597	1.14(−1)	3.08	4.52
0.600	0.657	1.21(−1)	3.28	4.46	0.600	0.543	1.19(−1)	3.14	4.50
					0.582	0.524	1.20(−1)	3.16	4.50‡
0.550	0.604	1.28(−1)	3.34	4.42	0.550	0.492	1.21(−1)	3.20	4.51
0.513	0.564	1.31(−1)	3.38	4.41‡					
0.500	0.549	1.32(−1)	3.40	4.41	0.500	0.443	1.21(−1)	3.28	4.53
0.450	0.493	1.33(−1)	3.48	4.44	0.450	0.396	1.20(−1)	3.36	4.58
0.400	0.436	1.30(−1)	3.57	4.50	0.400	0.351	1.15(−1)	3.47	4.66
0.350	0.378	1.23(−1)	3.68	4.60	0.350	0.308	1.09(−1)	3.59	4.77
0.300	0.321	1.13(−1)	3.81	4.75	0.300	0.265	9.96(−2)	3.75	4.94
0.250	0.265	9.85(−2)	3.98	4.99	0.250	0.223	8.75(−2)	3.94	5.17
0.200	0.209	8.03(−2)	4.22	5.34	0.200	0.182	7.23(−2)	4.19	5.51

Table III. Equilibrium sequences of the REs and the IRREs with $p=1$ and $\bar{a}/m_1=8$.

$p=1$									
$\bar{a}/m_1=8$									
Roche sequences					Irrotational Roche-Riemann Sequences				
a_3/a_1	a_2/a_1	$\tilde{\Omega}^2$	$\tilde{J}$	R/r_s	a_3/a_1	a_2/a_1	$\tilde{\Omega}^2$	$\tilde{J}$	R/r_s
0.950	0.968	2.02(−2)	3.82	11.00	0.950	0.947	3.04(−2)	3.56	9.71
0.900	0.932	3.95(−2)	3.61	8.98	0.900	0.890	5.53(−2)	3.37	8.13
0.850	0.894	5.78(−2)	3.54	8.03	0.850	0.830	7.54(−2)	3.30	7.44
0.800	0.853	7.50(−2)	3.51	7.46	0.800	0.769	9.13(−2)	3.28	7.06
					0.792	0.760	9.35(−2)	3.28	7.02†
0.774	0.830	8.34(−2)	3.51	7.24†					
0.750	0.809	9.09(−2)	3.51	7.07	0.750	0.709	1.04(−1)	3.29	6.84
0.700	0.762	1.05(−1)	3.53	6.81	0.700	0.651	1.13(−1)	3.31	6.70
0.650	0.712	1.17(−1)	3.56	6.63	0.650	0.595	1.20(−1)	3.36	6.62
0.600	0.661	1.27(−1)	3.60	6.51	0.600	0.541	1.24(−1)	3.42	6.59
					0.584	0.524	1.25(−1)	3.44	6.59‡
0.550	0.607	1.35(−1)	3.66	6.45	0.550	0.490	1.27(−1)	3.49	6.60
0.513	0.566	1.38(−1)	3.72	6.43‡					
0.500	0.552	1.39(−1)	3.74	6.44	0.500	0.441	1.27(−1)	3.59	6.64
0.450	0.495	1.40(−1)	3.83	6.48	0.450	0.394	1.25(−1)	3.70	6.72
0.400	0.438	1.37(−1)	3.94	6.57	0.400	0.349	1.20(−1)	3.83	6.85
0.350	0.380	1.30(−1)	4.08	6.74	0.350	0.306	1.13(−1)	3.99	7.03
0.300	0.322	1.18(−1)	4.26	6.99	0.300	0.264	1.04(−1)	4.19	7.29
0.250	0.265	1.03(−1)	4.49	7.37	0.250	0.223	9.06(−2)	4.45	7.66
0.200	0.210	8.33(−2)	4.80	7.94	0.200	0.181	7.47(−2)	4.78	8.22

Table IV. Equilibrium sequences of the REs and the IRREs with $p=0.1$ and $\bar{a}/m_1=3$.

$p=0.1$									
$\bar{a}/m_1=3$									
Roche Sequences					Irrotational Roche-Riemann Sequences				
a_3/a_1	a_2/a_1	$\tilde{\Omega}^2$	$\tilde{J}$	R/r_s	a_3/a_1	a_2/a_1	$\tilde{\Omega}^2$	$\tilde{J}$	R/r_s
					0.992	0.992	2.42(−3)	2.70	3.26†
0.990	0.992	2.39(−3)	2.71	3.27†					
0.950	0.959	9.94(−3)	2.85	2.35	0.950	0.949	1.17(−2)	2.89	2.27
0.900	0.914	1.80(−2)	3.02	2.08	0.900	0.896	2.04(−2)	3.06	2.03
0.850	0.868	2.51(−2)	3.16	1.96	0.850	0.843	2.76(−2)	3.19	1.93
0.800	0.821	3.12(−2)	3.26	1.88	0.800	0.789	3.35(−2)	3.29	1.86
0.750	0.772	3.65(−2)	3.35	1.84	0.750	0.735	3.84(−2)	3.37	1.82
0.700	0.722	4.10(−2)	3.42	1.80	0.700	0.682	4.23(−2)	3.43	1.79
0.650	0.672	4.47(−2)	3.48	1.78	0.650	0.629	4.53(−2)	3.48	1.77
0.600	0.621	4.75(−2)	3.52	1.76	0.600	0.577	4.74(−2)	3.51	1.76
0.550	0.569	4.93(−2)	3.56	1.75	0.550	0.526	4.86(−2)	3.54	1.76
					0.525	0.501	4.89(−2)	3.55	1.76‡
0.500	0.517	5.02(−2)	3.58	1.75‡	0.500	0.476	4.90(−2)	3.55	1.76
0.450	0.465	5.01(−2)	3.59	1.75	0.450	0.427	4.85(−2)	3.56	1.76
0.400	0.412	4.89(−2)	3.58	1.76	0.400	0.379	4.70(−2)	3.55	1.78
0.350	0.360	4.66(−2)	3.57	1.78	0.350	0.331	4.46(−2)	3.54	1.79

(continued)

0.300	0.308	4.29(−2)	3.54	1.81	0.300	0.284	4.11(−2)	3.51	1.82
0.250	0.255	3.80(−2)	3.49	1.85	0.250	0.238	3.64(−2)	3.46	1.86
0.200	0.204	3.17(−2)	3.42	1.92	0.200	0.192	3.05(−2)	3.40	1.93

Table V. Equilibrium sequences of the REs and the IRREs with $p=0.1$ and $\bar{a}/m_1=5$.

$p=0.1$									
$\bar{a}/m_1=5$									
Roche Sequences					Irrotational Roche-Riemann Sequences				
a_3/a_1	a_2/a_1	$\tilde{\Omega}^2$	$\tilde{J}$	R/r_s	a_3/a_1	a_2/a_1	$\tilde{\Omega}^2$	$\tilde{J}$	R/r_s
					0.962	0.961	1.10(−2)	2.71	3.28†
0.953	0.962	1.07(−2)	2.71	3.30†					
0.950	0.960	1.14(−2)	2.71	3.25	0.950	0.949	1.38(−2)	2.71	3.09
0.900	0.917	2.12(−2)	2.75	2.79	0.900	0.896	2.47(−2)	2.75	2.70
0.850	0.872	3.00(−2)	2.79	2.58	0.850	0.841	3.38(−2)	2.80	2.51
0.800	0.825	3.78(−2)	2.83	2.45	0.800	0.787	4.14(−2)	2.84	2.41
0.750	0.777	4.47(−2)	2.87	2.37	0.750	0.732	4.76(−2)	2.88	2.34
0.700	0.728	5.06(−2)	2.91	2.31	0.700	0.678	5.17(−2)	2.90	2.30
0.650	0.677	5.55(−2)	2.94	2.27	0.650	0.624	5.64(−2)	2.93	2.26
0.600	0.626	5.92(−2)	2.97	2.24	0.600	0.572	5.90(−2)	2.95	2.24
0.550	0.574	6.18(−2)	2.99	2.23	0.550	0.521	6.05(−2)	2.97	2.24
					0.528	0.498	6.08(−2)	2.98	2.24‡
0.500	0.521	6.30(−2)	3.00	2.22	0.500	0.471	6.09(−2)	2.98	2.24
0.497	0.518	6.31(−2)	3.00	2.22‡					
0.450	0.469	6.29(−2)	3.02	2.22	0.450	0.422	6.02(−2)	2.99	2.25
0.400	0.416	6.13(−2)	3.02	2.24	0.400	0.374	5.82(−2)	3.00	2.27
0.350	0.362	5.82(−2)	3.03	2.27	0.350	0.327	5.50(−2)	3.00	2.30
0.300	0.309	5.34(−2)	3.02	2.32	0.300	0.281	5.04(−2)	3.00	2.35
0.250	0.257	4.69(−2)	3.02	2.39	0.250	0.236	4.44(−2)	3.00	2.42
0.200	0.204	3.88(−2)	3.01	2.47	0.200	0.190	3.69(−2)	3.00	2.53

Table VI. Equilibrium sequences of the REs and the IRREs with $p=0.1$ and $\bar{a}/m_1=8$.

$p=0.1$									
$\bar{a}/m_1=8$									
Roche Sequences					Irrotational Roche-Riemann Sequences				
a_3/a_1	a_2/a_1	$\tilde{\Omega}^2$	$\tilde{J}$	R/r_s	a_3/a_1	a_2/a_1	$\tilde{\Omega}^2$	$\tilde{J}$	R/r_s
0.950	0.961	1.23(−2)	2.82	4.61	0.950	0.949	1.53(−2)	2.78	4.34
0.900	0.919	2.34(−2)	2.75	3.88	0.900	0.895	2.80(−2)	2.73	3.70
0.850	0.874	3.35(−2)	2.73	3.53	0.850	0.840	3.86(−2)	2.72	3.41
					0.849	0.840	3.87(−2)	2.72	3.41†
0.832	0.858	3.69(−2)	2.73	3.45†					
0.800	0.828	4.27(−2)	2.74	3.32	0.800	0.785	4.76(−2)	2.72	3.24
0.750	0.781	5.09(−2)	2.74	3.19	0.750	0.729	5.49(−2)	2.73	3.13
0.700	0.732	5.80(−2)	2.75	3.09	0.700	0.674	6.07(−2)	2.74	3.06
0.650	0.681	6.39(−2)	2.77	3.02	0.650	0.620	6.51(−2)	2.75	3.01
0.600	0.630	6.85(−2)	2.78	2.97	0.600	0.568	6.82(−2)	2.77	2.98

(continued)

0.550	0.578	7.17(−2)	2.79	2.95	0.550	0.516	6.99(−2)	2.78	2.97
					0.529	0.496	7.02(−2)	2.78	2.97‡
0.500	0.525	7.33(−2)	2.81	2.94	0.500	0.466	7.03(−2)	2.79	2.97
0.494	0.519	7.33(−2)	2.81	2.94‡					
0.450	0.472	7.32(−2)	2.82	2.94	0.450	0.418	6.93(−2)	2.81	2.98
0.400	0.418	7.13(−2)	2.84	2.97	0.400	0.371	6.69(−2)	2.82	3.02
0.350	0.364	6.75(−2)	2.85	3.02	0.350	0.324	6.31(−2)	2.84	3.07
0.300	0.311	6.17(−2)*	2.87	3.09	0.300	0.279	5.76(−2)	2.86	3.14
0.250	0.258	5.39(−2)	2.90	3.21	0.250	0.234	5.05(−2)	2.89	3.26
0.200	0.205	4.41(−2)	2.93	3.38	0.200	0.189	4.17(−2)	2.93	3.44

A. $p=1$ *case*

Figure 2(a) shows $\tilde{J}$ as a function of the normalized separation R/r_s. In (a), thin solid, dotted and dashed lines are the REs with $\bar{a}/m_1$ being 3, 5 and 8, respectively, while thick solid, dotted and dashed lines are the IRREs with $\bar{a}/m_1$ being 3, 5 and 8, respectively. We defined in § 2.C that the location of the ISCO is the minimum point of $\tilde{J}$. From Fig. 2(a), we see that the separations of the binary at the ISCO in the IRREs case are almost the same as those in the REs case.

Figure 2(b) shows the axial ratios a_2/a_1 and a_3/a_1 as functions of R/r_s. The conventions of lines are the same as those in (a). The relation among the length of the axes is $a_1>a_2>a_3$ in the REs, while $a_1>a_3>a_2$ in the IRREs. In the REs, the tidal force makes the a_1 axis long while it does a_2 and a_3 axes short. The centrifugal force makes a_1 and a_2 axes long. As a result, we have $a_1>a_2>a_3$. In the IRREs, in

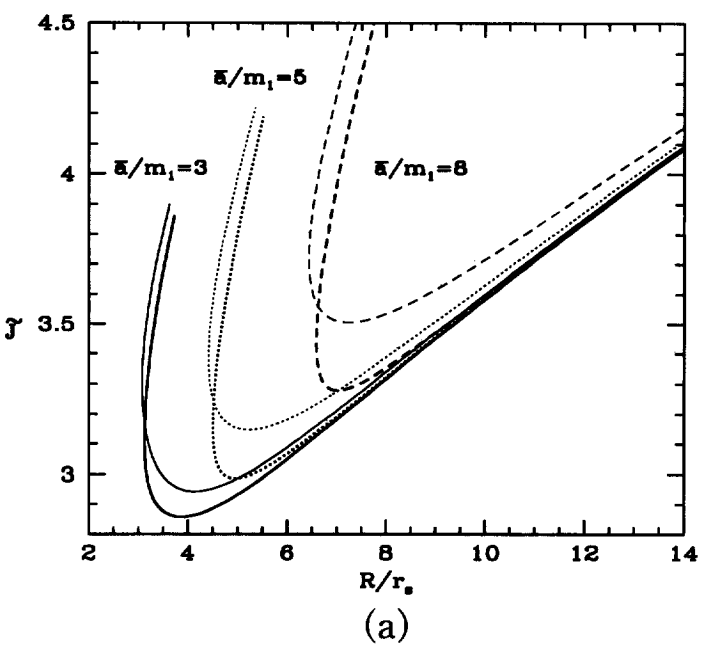

Fig. 2. (continued)

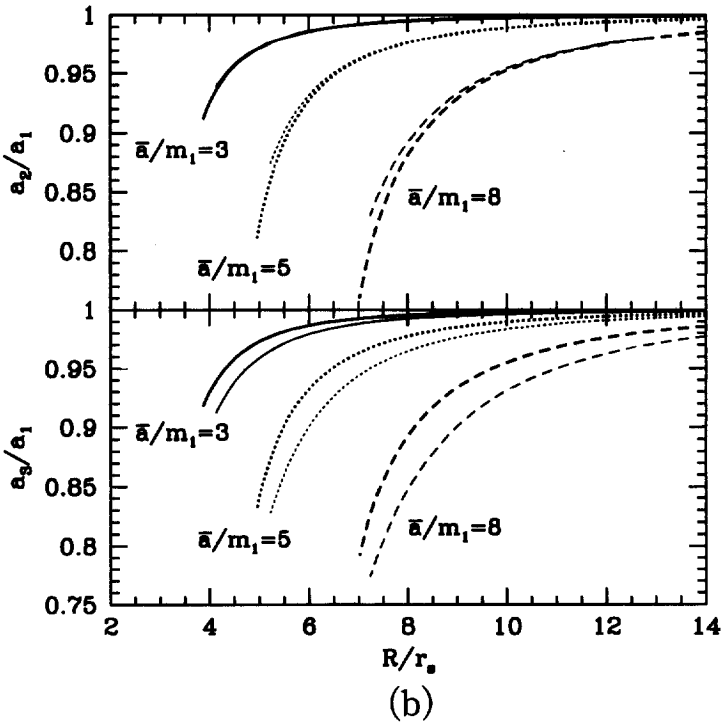

Fig. 2. (a) The total angular momentum $\tilde{J}=J_{\rm tot}/\{m_1m_2(r_s/M_{\rm tot})^{1/2}\}$ of the equilibrium sequence as a function of R/r_s in the case that the mass ratio is $p=1$. Thin and thick lines express the REs and the IRREs cases, respectively. Solid, dotted and dashed lines denote $\bar{a}/m_1=3$, 5 and 8, respectively. (b) The axial ratios a_2/a_1 and a_3/a_1 of the equilibrium sequence as a function of R/r_s in the case of the mass ratio $p=1$. The top figure represents a_2/a_1, and the bottom does a_3/a_1. The conventions are the same as in (a).

addition to the above effects, the Coriolis force caused by the internal motion of the primary exists. This makes a_1 and a_2 axes short, which yields $a_1>a_3>a_2$.

From Fig. 2(b), it is found that in the IRREs the star with $\bar{a}/m_1=3$ reaches the ISCO at the point of $a_2/a_1\simeq0.912$ and $a_3/a_1\simeq0.918$. On the other hand, the star with $\bar{a}/m_1=8$ terminates when $a_2/a_1\simeq0.760$ and $a_3/a_1\simeq0.792$. This means that the primary with a smaller mean radius reaches the ISCO before the shape of the primary deviates from the sphere considerably. This tendency is the same for the REs.

B. $p=0.1$ *case*

Figure 3(a) shows $\tilde{J}$ as a function of R/r_s. The conventions are the same as those in Fig. 2(a). From Fig. 3(a), we see that all lines with the mean radii in the range $3\leq\bar{a}/m_1\leq8$ take their minima at points near $R/r_s\sim3.25$. This value is almost the same as the ISCO by Kidder, Will and Wiseman[7] for $p=0.1$. This means that when p is much less than 1 and the mean radius of the primary is less than $8m_1$, which corresponds to 17 km for $m_1=1.4M_\odot$, the size of the primary has little effect on the ISCO.

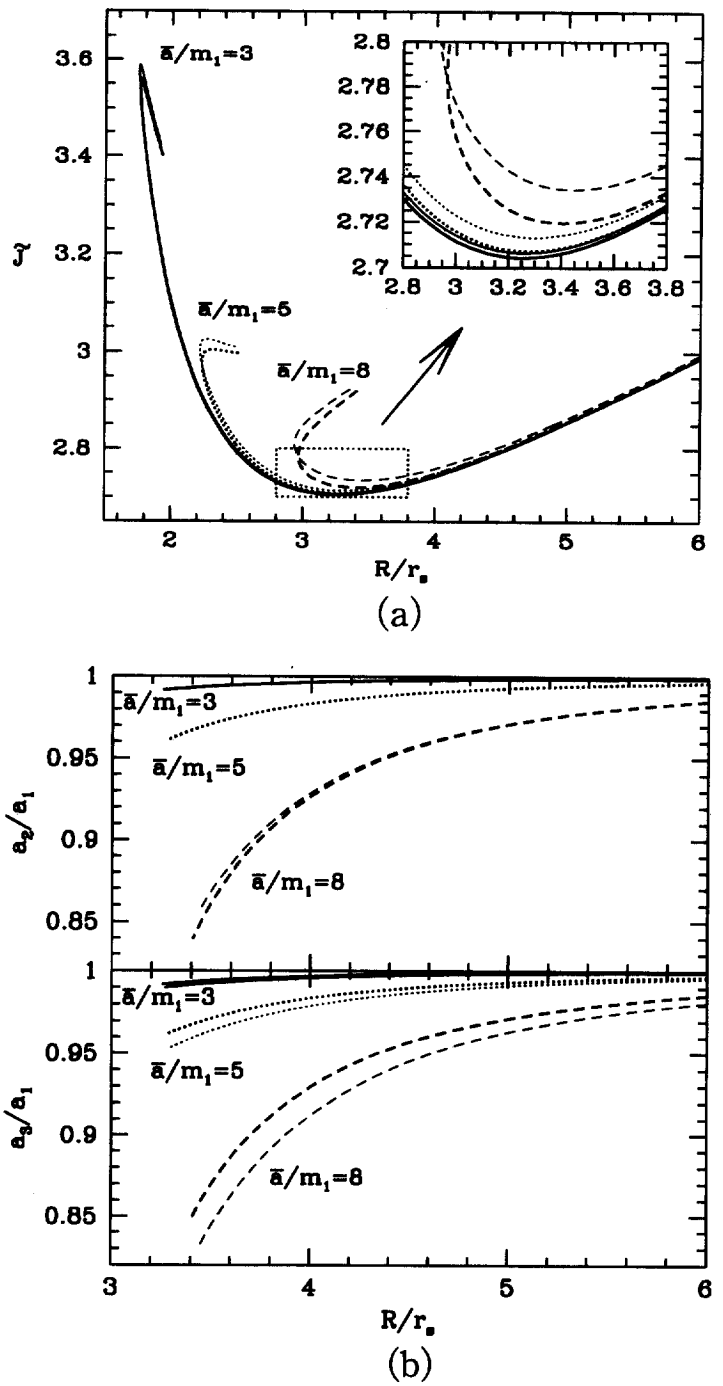

Fig. 3. (a) The total angular momentum $\tilde{J}$ of the equilibrium sequence as a function of R/r_s in the case $p=0.1$. The region around the minimum of the lines is magnified and shown in the upper right corner. The conventions are the same as in Fig. 2(a). (b) The axial ratios a_2/a_1 and a_3/a_1 of the equilibrium sequence as a function of R/r_s in the case $p=0.1$. The top figure represents a_2/a_1, and the bottom does a_3/a_1. The conventions are the same as in Fig. 2(a).

Figure 3(b) shows the axial ratios a_2/a_1 and a_3/a_1 as a function of R/r_s. The conventions are the same as those in Fig. 3(a). We see that stars with smaller mean radii reach the ISCO even when the deviation from the spherical symmetry is very small. Since the binary system enters an unstable circular orbit before the primary is tidally deformed, tidal effects are not important. We see that even when $\bar{a}/m_1 \sim 8$ the minimum values a_2/a_1 and a_3/a_1 are not small (~ 0.85).

§ 5. Discussion

In this section, we discuss the differences between the case of the generalized pseudo-Newtonian potential and that of the Newtonian potential, and between the REs and the IRREs. We also compare our results with other papers.

A. *The case* $p=1$

In Fig. 4, the separation $R_{\rm ISCO}/r_s$ is shown as a function of $\bar{a}/m_1$. Thick lines and thin lines represent the case of the generalized pseudo-Newtonian potential and that of the Newtonian potential, respectively. Solid lines and dotted lines express the case of the IRREs and the REs, respectively. We see that for the Newtonian potential, $R_{\rm ISCO}/r_s$ increases in proportion to $\bar{a}/m_1$ regardless of types of ellipsoids, while for the generalized pseudo-Newtonian potential, the behavior of $R_{\rm ISCO}/r_s$ changes around $\bar{a}/m_1 \simeq 3.5$.

For $\bar{a}/m_1 \gtrsim 3.5$, $R_{\rm ISCO}/r_s$ increases in proportion to $\bar{a}/m_1$ as in the case of the Newtonian potential. In this region, the tidal effect dominates the system, and the

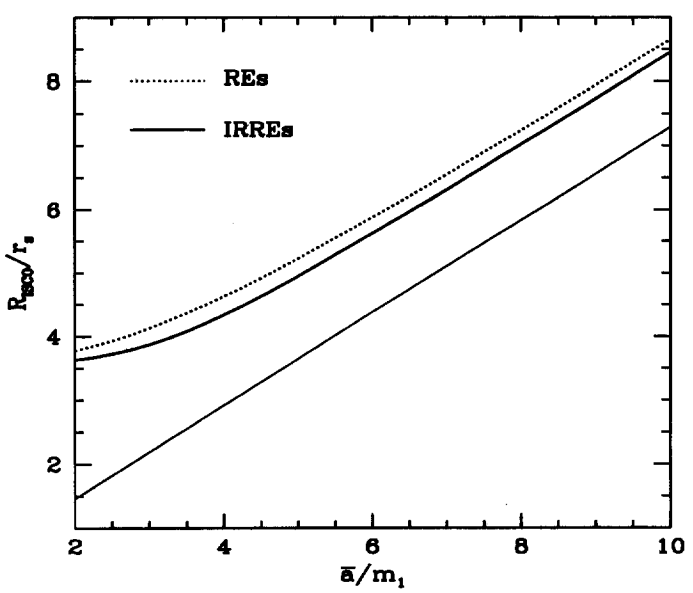

Fig. 4. The relation between the mean radius of the primary $\bar{a}/m_1$ and the separation of the binary $R_{\rm ISCO}/r_s$ at the ISCO in the case $p=1$. Thin lines denote the case of the Newtonian potential as an interaction potential, and thick lines denote the case of the generalized pseudo-Newtonian potential. The solid and dotted lines represent the IRREs and the REs, respectively.

effects of general relativity become less important. In conclusion, for $\bar{a}/m_1 \gtrsim 3.5$, the tidal effect dominates the stability of the binary system and for $\bar{a}/m_1 \lesssim 3.5$, the binary system is dominated by the relativistic effect, i.e., the fact that the interaction potential has an unstable orbit. From Fig. 4 it is also found that the location of the ISCOs in the IRREs case is not so different from that in the REs case for the same $\bar{a}/m_1$.

The orbital frequency of the IRREs at the ISCO for $m_1=1.4M_\odot$ and $\bar{a}/m_1=5$ is estimated from $\tilde{\Omega}$ in Table IV as

$$\Omega_{\rm ISCO}=495\,[{\rm Hz}]\,. \tag{5·1}$$

This value is smaller than that in the Newtonian potential case ($\Omega_{\rm ISCO}^{\rm Newton}=599\,[{\rm Hz}]$).

B. *The case* $p=0.1$

If we consider the primary as a neutron star of mass $1.4M_\odot$, then, the secondary is regarded as a black hole of mass $14M_\odot$. $R_{\rm ISCO}/r_s$ is shown as a function of $\bar{a}/m_1$ in Fig. 5. For the Newtonian potential, $R_{\rm ISCO}/r_s$ increases in proportion to $\bar{a}/m_1$ as in the case $p=1$. For the generalized pseudo-Newtonian potential, in the range of $\bar{a}/m_1$ of Fig. 5, $R_{\rm ISCO}/r_s$ converges to the value 3.25 obtained by Kidder, Will and Wiseman.[7] This is because the existence of the unstable orbit in the generalized pseudo-Newtonian potential influences $R_{\rm ISCO}/r_s$, and this effect dominates when the radius of the primary is small. This is clearer for a small mass ratio p. Therefore if p is small, for the range of the radius ($3\lesssim \bar{a}/m_1 \lesssim 8$) relevant to the neutron star, the effect of the neutron star's size is very small. This comes essentially from the fact that the Newtonian estimate of the Roche radius is smaller than the radius of the ISCO.

One can estimate the orbital frequency of the IRREs at the ISCO for $m_1=1.4M_\odot$

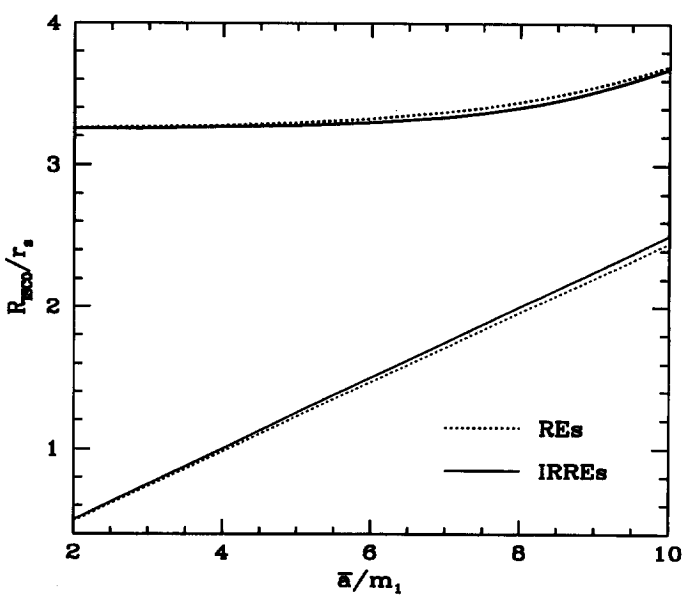

Fig. 5. The relation between the mean radius of the primary $\bar{a}/m_1$ and the separation of the binary $R_{\rm ISCO}/r_s$ at the ISCO in the case $p=0.1$. The conventions are the same as in Fig. 4.

and $\bar{a}/m_1=5$ from $\tilde{\Omega}$ in Table *V* as

$$\Omega_{\rm ISCO}=187\,[{\rm Hz}]\,. \tag{5·2}$$

C. Comparison with other works

Kidder, Will and Wiseman[7] studied the motion of point-particle binary systems using *a hybrid Schwarzschild second post-Newtonian equation of motion*, and obtained the separation at the ISCO ($r_{\rm ISCO}$) expressed by

$$\frac{r_{\rm ISCO}}{M_{\rm tot}}\simeq 6+7.49\eta-20.8\eta^2+29.3\eta^3\,, \tag{5·3}$$

where

$$\eta=\frac{m_1m_2}{M_{\rm tot}^2}\,. \tag{5·4}$$

Table VII shows the comparison of Eq. (5·3) with our results for $\bar{a}/m_1=5$. It is found that for $p=0.1$, the finite size effect is not important, because the primary is much lighter than the secondary, so that the results are almost the same as Ref. 7). On the other hand, when $p=1$, the finite size of the primary increases the separation at the ISCO by the general relativistic and tidal effects.

Lai, Rasio and Shapiro,[18] discussed relativistic effects on the binary system for compressible Darwin ellipsoids using a simple approximate model.[19] The Darwin ellipsoids are the equilibrium configurations constructed by two identical synchronized finite-size stars, including mutual tidal interactions. In their approach the effects of general relativity and the Newtonian tidal interactions for finite-size compressible stars are combined by hand. While we formulated the problem using arbitrary interaction potentials of the secondary for the incompressible primary. We adopted the semi-relativistic potential called the generalized pseudo-Newtonian potential to mimic the general relativistic effects of gravitation. We solved the equilibria of the

Table VII. Comparison of our results ($\bar{a}/m_1=5$) with those of Kidder, Will and Wiseman[7] in the cases $p=1$ and 0.1.

	p	0.1	1
results of Ref. 7)	$r_{\rm ISCO}/M_{\rm tot}$	6.5	7.0
Our results	$R^{\rm RE}_{\rm ISCO}/M_{\rm tot}$	6.6	10.4
Our results	$R^{\rm IRRE}_{\rm ISCO}/M_{\rm tot}$	6.6	9.9

Table VIII. Comparison of our results ($p=1$) with those of Lai, Rasio and Shapiro[18] in the cases $\bar{a}/m_1=5$ and 8.

$p=1$			
	$\bar{a}/m_1$	5	8
results of Ref. 18)	$r_m/M_{\rm tot}$	8.5	12
Our results	$R^{\rm RE}_{\rm ISCO}/M_{\rm tot}$	10.4	14.5
Our results	$R^{\rm IRRE}_{\rm ISCO}/M_{\rm tot}$	9.9	14.0

REs and the IRREs in this potential. Their results and ours are compared in Table VIII, where r_m expresses the minimum separation obtained by Lai, Rasio and Shapiro.[18] From this table, we see that the results agree rather well inspite of the different approaches and approximations.

Acknowledgements

KT would like to thank H. Sato, K. Nakao and M. Shibata for useful discussions and continuous encouragement. This work was in part supported by a Grant-in-Aid for Basic Research of Ministry of Education, Culture, Science and Sports (08NP0801).

References

1) A. Abramovici et al. Science **256** (1992), 325.
2) C. Bradaschia, et al. Nucl. Instrum. and Methods **A289** (1990), 518.
3) J. Hough, in *Proceedings of the Sixth Marcel Grossmann Meeting*, ed. H. Sato and T. Nakamura (World Scientific, Singapore, 1992), p. 192.
4) K. Kuroda et al. in *Proceedings of International Conference on Gravitational Waves: Sources and Detectors,* Pisa, Italy, March 19-23, 1996 (in press).
5) C. Cutler and E. E. Flanagan, Phys. Rev. **D49** (1994), 2658.
6) C. Cutler et al. Phys. Rev. Lett. **70** (1993), 2984.
7) L. E. Kidder, C. M. Will and A. G. Wiseman, Class. Quantum Gravity **9** (1992), L125.
L. E. Kidder, C. M. Will and A. G. Wiseman, Phys. Rev. **D47** (1993), 3281.
8) S. Chandrasekhar, Ellipsoidal Figures of Equilibrium (Yale University Press, New Haven, 1969).
9) D. Lai, F. A. Rasio and S. L. Shapiro, Astrophys. J. Suppl. **88** (1993), 205.
10) D. Lai, F. A. Rasio and S. L. Shapiro, Astrophys. J. **423** (1994), 344.
D. Lai, F. A. Rasio and S. L. Shapiro, Astrophys. J. **437** (1994), 742.
11) T. Nakamura, in *Proceedings of the Seventh Marcel Grossmann Meeting,* Stanford, July, 1994 (in press).
12) J. R. Wilson and G. J. Mathews, Phys. Rev. Lett. **75** (1995), 4161.
J. R. Wilson, G. J. Mathews and P. Marroetti, gr-qc/9601017 (1996).
13) M. Shibata, Osaka University Preprint OU-TAP 26 (1995).
M. Shibata, Prog. Theor. Phys. **96** (1996), 317.
14) B. Paczyfisky and P. J. Wiita, Astron. Astrophys. 88 (1980), 23.
15) M. L. Aizenman, Astrophys. J. **153** (1968), 511.
16) C. S. Kochanek, Astrophys. J. **398** (1992), 234.
17) L. Bildsten and C. Cutler, Astrophys. J. **400** (1992), 175.
18) D. Lai, F. A. Rasio and S. L. Shapiro, Astrophys. J. **420** (1994), 811.
19) D. Lai, F. A. Rasio and S. L. Shapiro, Astrophys. J. **406** (1993), L63.